

Localized Traveling-Wave Convection in Binary-Fluid Mixtures

W. Barten,⁽¹⁾ M. Lücke,⁽¹⁾ and M. Kamps⁽²⁾

⁽¹⁾*Institut für Theoretische Physik, Universität des Saarlandes, D-6600 Saarbrücken, Federal Republic of Germany*

⁽²⁾*Stabsstelle Supercomputing, Forschungszentrum Jülich, D-5170 Jülich, Federal Republic of Germany*
(Received 13 August 1990)

The structure and dynamics of both subcritical and supercritical localized traveling-wave (LTW) convective states with different extensions and uniquely selected width are determined by numerical integration of the proper hydrodynamic field equations with realistic horizontal boundary conditions. A large-scale mean concentration current loop influences the LTW significantly. It generates a concentration distribution that hinders propagation of the LTW pulse, so that the group velocity is small but finite.

PACS numbers: 47.25.Qv, 47.20.-k, 47.35.+i

Traveling-wave (TW) phenomena appear in many linear and nonlinear systems. An example of the latter are TW patterns of convective rolls in binary-fluid mixtures heated from below. This nonequilibrium system is experimentally and theoretically very well suited to study nonlinear pattern dynamics. Recently, spatially confined states of localized traveling-wave (LTW) convective rolls have been found¹⁻⁵ in this system. Looking like wave packets that result from linear superpositions of TW's, these LTW's are nonlinear phenomena. They consist of traveling patterns of straight rolls that are localized laterally, i.e., perpendicular to the roll axes, by intensity envelopes which drop to zero into the surrounding quiescent conductive state via a leading and a trailing front. There are subcritical and supercritical LTW states below and above, respectively, the bifurcation threshold for onset of extended convection. Depending on initial conditions and driving history the system either ends up in a LTW or an extended state filling the whole space. Depending on the parameters, the extended states competing with the LTW are the basic conductive state, TW convection, or stationary convection. For certain parameters a multiplicity of LTW's with different lateral widths are stable^{1,4} while for others the LTW pulse and its width are uniquely selected.²

Many features of these LTW states are not understood. Our numerical simulations reveal that the LTW fields are not just pulses of harmonic waves with a common simple envelope. Furthermore, LTW's with different and uniquely selected widths differ only in their center parts while the leading and trailing fronts and the field structure under the respective fronts are the same. Here we provide the information lacking so far on the concentration fields and currents that play a very important role. In particular, we find in all LTW's a feedback mechanism between the LTW fields and a large-scale mean lateral concentration current loop. This interplay leads to a concentration distribution ahead of the pulse which hinders its propagation and decreases the group velocity from the large value of simple Ginzburg-Landau approaches⁶ to almost zero, in agreement with experi-

mental observations.

Our results follow from numerically solving the hydrodynamic field equations as described elsewhere^{7,8} in an x - z section of the layer with rigid, isothermal, impermeable horizontal boundaries at $z=0, d$ and periodic boundaries at $x=0$ and $20d$, where d is the layer thickness. The fluid parameters,⁹ Lewis number $L=D/\kappa=0.01$ and Prandtl number $\sigma=\nu/\kappa=10$, are typical for room-temperature ethanol-water mixtures. Here D is the concentration diffusion constant, κ the thermal diffusivity, and ν the kinematic viscosity. We measure lengths in units of d and time in units of the vertical thermal diffusion time d^2/κ . Temperatures T are reduced by the applied temperature difference ΔT between top and bottom, and concentration C by $\Delta T\alpha/\beta$, where $\alpha=(-1/\rho)\partial\rho/\partial T$ and $\beta=-(1/\rho)\partial\rho/\partial C$ are thermal and solutal expansion coefficients, respectively.

In the quiescent, laterally homogeneous conductive state the temperature and concentration variation around the mean T_0, C_0 ,

$$\begin{aligned} T_{\text{cond}}(z) &= T_0 - (z - \frac{1}{2}), \\ C_{\text{cond}}(z) &= C_0 - \psi(z - \frac{1}{2}), \end{aligned} \quad (1)$$

generates the vertical buoyancy force $b_{\text{cond}}(z) = -\sigma R \times (1 + \psi)(z - \frac{1}{2})$ that drives convection. Its magnitude, which increases linearly with Rayleigh number R , is reduced for negative separation ratios ψ (Ref. 9) via the Soret effect. We shall use $r = R/R_c^0$ as a control parameter measuring the driving force, with R_c^0 denoting the convective onset in a pure fluid ($\psi=0$). For negative ψ there is, at a threshold r_{osc} , a backwards Hopf bifurcation of the conductive state into an unstable extended state of TW convection. This unstable branch turns forward at a saddle point r_{TW}^* into an upper stable TW branch (Fig. 1, bottom). At r_{osc} the TW frequency is given by the Hopf frequency ω_H . Then ω decreases monotonically when following the TW solution via the saddle to the upper stable branch (Fig. 1, top). Finally, the TW merges at r^* with zero frequency into a branch of stationary overturning convection (SOC) states (solid

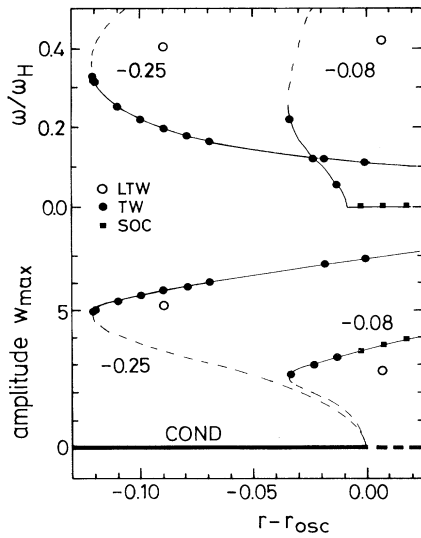


FIG. 1. Positions of LTW states (open circles) discussed here in the bifurcation diagrams of frequency ω and of maximal vertical flow velocity w_{\max} vs Rayleigh number for $\psi = -0.25, -0.08$. Solid symbols are numerically obtained extended states. Thin lines are guides to the eye. Schematic dashed lines for unstable TW branches show the bifurcation topology (Ref. 10). For $L=0.01$, $\sigma=10$, and $\psi = -0.25, -0.08$ the oscillatory threshold (Ref. 11) is at $r_{\text{osc}}=1.3347, 1.0965$; Hopf frequency (Ref. 11) $\omega_H=11.235, 5.753$; group velocity of linear TW (Ref. 12) at onset $v_g^c \approx \omega_H/\pi$; TW saddle point (Ref. 8) $r_{\text{TW}}^c \approx 1.215, 1.06$; transition TW \leftrightarrow SOC (Ref. 8) $r^* \approx 1.65, 1.09$. Our LTW's are at $r - r_{\text{osc}} = -0.089, 0.008$.

squares in Fig. 1) that become stable for $r > r^*$.⁸

We present here LTW solutions (open circles in Fig. 1) at a subcritical driving for $\psi = -0.25$ and at a supercritical driving for $\psi = -0.08$. The maximum LTW flow amplitudes w_{\max} are slightly smaller while the frequencies are considerably larger than those in the extended states at the same r . For $\psi = -0.25$ we have evaluated three different LTW's at the same Rayleigh number having widths $l \approx 6.5, 8.9$, and 9.9 but very similar ω and w_{\max} . Also, the structure of the fields under the fronts of these LTW pulses is the same, with only the center part of the different LTW's differing slightly. Our simulations indicate that there exist LTW's with many different widths. A multiplicity of LTW states was also found experimentally^{1,4} for $\psi = -0.25$. However, despite applying various search procedures for $\psi = -0.08$ we found only one LTW. Its width $l \approx 4.9$ agrees with the experimental result of Niemela, Ahlers, and Cannell.² All LTW's move in the direction of phase propagation with a small group velocity v_g that is smaller than the group velocity v_g^c of linear TW's at onset by a factor of ≈ 70 for $\psi = -0.25$ (35 for $\psi = -0.08$).¹² Furthermore, v_g is smaller than the mean phase velocity of the LTW by a factor of ≈ 30 for $\psi = -0.25$ (15 for $\psi = -0.08$).

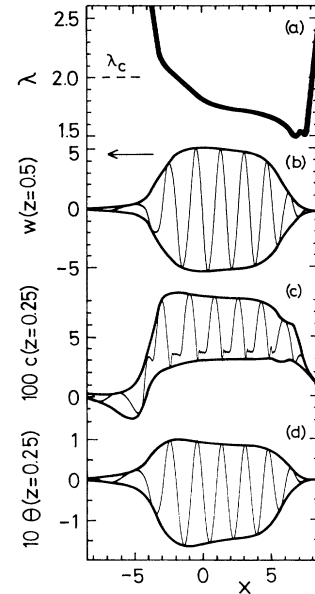


FIG. 2. Lateral structure of the LTW state $\psi = -0.25$, $r=1.246$, $\omega=4.525$, $v_g=0.051$, width 8.9 . Phase and group velocity is to the left, as indicated by the arrow. The local wavelength is shown in (a) together with the critical one λ_c . Thin lines in (b)–(d) show snapshots of w , c , and θ fields at different vertical positions and thick lines show the pulse envelopes along which the extrema move during one oscillation period. The origin of the abscissa is chosen arbitrarily.

Figure 2 shows the lateral structure of the LTW in snapshots of the local wavelength $\lambda(x)$, the vertical flow velocity w , and the convective concentration and temperature fields

$$c = C - C_{\text{cond}}, \quad \theta = T - T_{\text{cond}}. \quad (2)$$

Under the leading front the wavelength determined from monitoring the node distances of w over one oscillation period is larger than the critical one λ_c . Then it decreases^{1,2,4} towards the pulse center to values $\lambda < \lambda_c$ and tends to become plateaulike before it drops even further under the trailing front. The LTW's at $\psi = -0.25$, $r = 1.246$ having different widths have *identical* λ profiles under the fronts—only the center parts differ.

The fields $f = u, w, c, \theta$ are time periodic with period τ in the reference frame $\tilde{\Sigma}$ comoving with the group velocity. They display the symmetry

$$\tilde{f}_{\text{LTW}}(\tilde{x}, z; t) = \pm \tilde{f}_{\text{LTW}}(\tilde{x}, 1 - z; t + \tau/2) \quad (3)$$

under time translation by $\tau/2$ combined with vertical reflection at the midplane of the layer, with $+$ for u and $-$ for w , θ , and c . The extended TW shows this symmetry in the laboratory frame and, in addition, the symmetry^{7,8} $f_{\text{TW}}(x, z; t) = \pm f_{\text{TW}}(x + \lambda/2, 1 - z; t)$ that is broken by the lateral intensity variation of the LTW. In the center part of the LTW the fields are very similar to

those in an extended TW with similar ω —compare, e.g., the laterally highly anharmonic c -field variation of a TW (Refs. 7 and 8) and LTW. The latter differs drastically from the variation $\sim e^{ikx}$ of linear TW's. Furthermore, since the c pulse differs substantially from the w and θ pulses, the LTW state is not just a wave packet, $\sim A(x)e^{ikx}$, with one single smooth envelope $A(x)$. Recent measurements by Surko *et al.*⁴ of the shadowgraph intensity structure $I(x)$ of pulses at $\psi = -0.258$ agree very well with our numerical predictions for $I(x)$.⁴

The pulse envelopes [thick lines in Figs. 2(b)–2(d)] were found by superimposing graphs at several times during one period τ . The envelopes translate within time τ only by a distance ≈ 0.07 that cannot be resolved in Fig. 2. This slow group velocity of the pulse was determined from the spatial moments of w^2 . A control run in a system with extension 40 showed that a minute head-tail overlap of the c pulse in the smaller system does not play a role. Note the different shapes and extensions of the w , c , and θ pulse envelopes. They are to a varying degree asymmetric around the center: The leading front is steeper than the trailing one and the amplitude is largest just behind the leading front.

Figure 3 shows the time averages $\langle c \rangle$ and $\langle \theta \rangle$ of the fields of Figs. 2(c) and 2(d) over one oscillation period. In a TW these averages^{7,8,13} are constant in x giving,

e.g., the $k_x = 0$ mode of θ that carries the vertical convective heat current. The spatial form of the averaged fields suggests a simple physical explanation for the puzzle of why the pulses do not propagate with the fast group velocity v_g^c as suggested by simple *ad hoc* Ginzburg-Landau approaches⁶ but rather are almost stationary. In fact, in the experimental annular channels^{1–4} the pulses are, after transients, completely at rest.¹⁴

Here we present an intrinsic mechanism that is not contained in the Ginzburg-Landau equation and that strongly *hinders* the pulse propagation. The phase difference between c and w in the center part of the LTW generates¹³ as in an extended TW a strong, primary large-scale, mean concentration current^{7,8}

$$\langle \mathbf{J} \rangle = \langle (C - C_0) \mathbf{u} \rangle - L \nabla \langle C - \psi T \rangle \quad (4)$$

that flows in the upper (lower) half of the layer parallel (antiparallel) to the phase and group velocity and which is the key mechanism for creating a special $\langle c \rangle$ distribution. Except for a narrow spatial range under the fronts $\langle \mathbf{J} \rangle$ is dominated by the first convective contribution to (4). The current is deflected vertically under the fronts of the pulse to form a large primary concentration circulation loop [dashed lines in Fig. 3(b)] since in the conductive state there can be no concentration current. Under the leading (trailing) front the vertical current $\langle J_z \rangle$ is laterally focused (dilated). Since part of $\langle J_z \rangle$ is diffusive under the fronts and since the θ pulse is narrower than the c pulse [cf. Fig. 3(c)], the associated mean vertical concentration gradient around midheight of the layer is bigger (smaller) under the leading (trailing) front than in the conductive state. So the current sustains, relative to the conductive concentration stratification, a small concentration surplus (deficiency) in the upper (lower) half of the layer just ahead of the leading front as shown by the thin isolines of $\langle c \rangle$ in Fig. 3(a). In this transition region from conduction to convection, the above concentration difference generates at the plates a diffusive lateral current $-L \partial_x \langle c \rangle$. While at the trailing front it strengthens the large primary concentration loop, it is directed under the leading front opposite to the primary current, thus generating two small secondary countercirculating current loops [solid lines in Fig. 3(b)] under the leading front.

Thus the net overall effect of the primary lateral current that is generated in the center part of the pulse and that transports concentration to (away from) the leading front is to deposit (withdraw) concentration in the region ahead of the leading front in the upper (lower) half of the layer. The resulting concentration distribution ahead of the leading front stabilizes the conductive state and hinders convection since the convective contribution $\langle b - b_{\text{cond}} \rangle = \sigma R \langle c + \theta \rangle$ reduces the size of the mean buoyancy force. The negative dip in the thick solid line in Fig. 3(c) showing $\langle c + \theta \rangle$ at $z = \frac{1}{4}$ demonstrates the vertically downwards, i.e., stabilizing, contri-

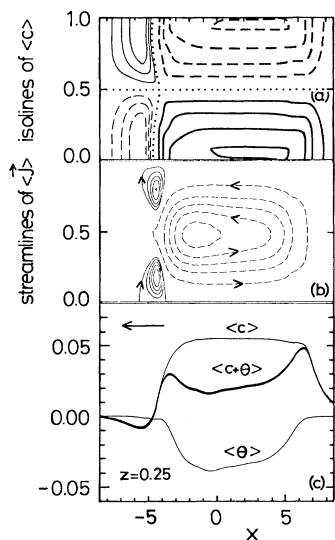


FIG. 3. Time averages over one oscillation period of the LTW of Fig. 2. In (a) thick (thin) isolines of $\langle c \rangle$ are shown in the x - z plane with increment 0.02 (0.002). Solid (dashed) lines mark positive (negative) $\langle c \rangle$. Dots show $\langle c \rangle = 0$. In (b) streamlines of the mean concentration current $\langle \mathbf{J} \rangle$ are shown by dashed (solid) lines for the large-scale, large-amplitude primary (small-amplitude secondary) current loops. For better presentation the stream-function scale has been magnified for the solid lines. In (c) the lateral profiles of $\langle c \rangle$ and $\langle \theta \rangle$ are shown at $z = 0.25$ together with $\langle c + \theta \rangle$ determining the convective contribution to the mean buoyancy force.

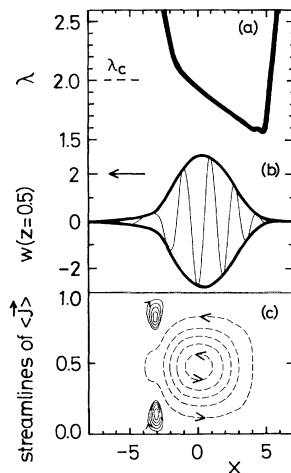


FIG. 4. The supercritical LTW at $\psi = -0.08$, $r = 1.104$ ($\omega = 2.425$, $v_g = 0.052$, width 4.9). (a) Local wavelength. (b) Snapshot and envelope of w as in Figs. 2(a) and 2(b). (c) Streamlines of $\langle c \rangle$ as in Fig. 3(b).

tribution to $\langle b \rangle$ in the lower half of the layer. Similarly, in the upper half, $\langle c + \theta \rangle$ is positive, so that again the convective contribution is stabilizing, i.e., upwards. In the center part of the pulse, on the other hand, $\langle c \rangle$ enhances the conductive driving force.

In Fig. 4 we show for $\psi = -0.08$ the uniquely selected LTW at the slightly supercritical driving $r - r_{\text{osc}} = 0.008$. Note, however, the latter's similarity to the previously described subcritical ones. The variation of $\lambda(x)$ [Fig. 4(a)] is almost identical to that of Fig. 2(a) except for the plateaulike center part of the wider subcritical pulse. Also, the streamlines of $\langle \mathbf{J} \rangle$ in Fig. 4(c) reveal the same concentration transport mechanism as in subcritical LTW's. In a sense the narrow uniquely selected LTW at $\psi = -0.08$ consists only of two fronts without the center part of the wider LTW's at $\psi = -0.25$.

The existence of supercritical pulses which do not expand to fill the entire system seems to be related to the conductive state being only convectively but not absolutely unstable.¹⁵ In our laterally periodic system and in experimental annuli¹⁻⁴ small perturbations of the conductive state are convectively swept into the pulse with the fast linear group velocity $\approx v_g^c$ thus allowing a coexistence of localized convection and conduction.

Our numerical analysis of pulselike nonlinear LTW convection done for the basic fields of velocity, temperature, and concentration has given insights into many puzzling¹⁻⁶ problems: The field and wavelength variations

under the respective fronts of pulses of variable and uniquely selected width are almost identical. Basically only the center-part extension of the LTW's differ. The pulses do not move with the fast group velocity of a superposition of linear TW's. They are slowed down to almost zero by a global, pulse-induced concentration redistribution. This is an example of an intrinsic feedback in a nonequilibrium system between the structural dynamics of a confined pattern and a large-scale current generated by the latter.

We are grateful to G. Ahlers, P. Kolodner, D. R. Ohlsen, and C. M. Surko for helpful conversations. Support by the Deutsche Forschungsgemeinschaft and by the Stiftung Volkswagenwerk is acknowledged by W.B. and M.K., respectively.

¹P. Kolodner, D. Bensimon, and C. M. Surko, Phys. Rev. Lett. **60**, 1723 (1988); D. Bensimon *et al.*, J. Fluid Mech. **217**, 441 (1990).

²J. J. Niemela, G. Ahlers, and D. S. Cannell, Phys. Rev. Lett. **64**, 1365 (1990).

³K. E. Anderson and R. P. Behringer, Phys. Lett. A **145**, 323 (1990).

⁴C. M. Surko, D. R. Ohlsen, S. Y. Yamamoto, and P. Kolodner, Phys. Rev. A (to be published).

⁵R. Heinrichs, G. Ahlers, and D. S. Cannell, Phys. Rev. A **35**, 2761 (1987); E. Moses, J. Fineberg, and V. Steinberg, *ibid.* **35**, 2757 (1987).

⁶S. Fauve and O. Thual, Phys. Rev. Lett. **64**, 282 (1990); W. van Saarloos and P. C. Hohenberg, *ibid.* **64**, 749 (1990), and references cited in these works.

⁷W. Barten, M. Lücke, W. Hort, and M. Kamps, Phys. Rev. Lett. **63**, 376-379 (1989).

⁸W. Barten, M. Lücke, and M. Kamps, in *Nonlinear Evolution of Spatiotemporal Structures in Dissipative Continuous Systems*, edited by F. Busse and L. Kramer, NATO Advanced Study Institute, Ser. B2, Vol. 225 (Plenum, New York, 1990), p. 131.

⁹P. Kolodner, H. Williams, and C. Moe, J. Chem. Phys. **80**, 6512 (1988).

¹⁰D. Bensimon, A. Pumir, and B. I. Shraiman, J. Phys. (Paris) **50**, 3089 (1989).

¹¹W. Hort, Diplomarbeit, Universität Saarbrücken, 1990 (unpublished).

¹²M. C. Cross and K. Kim, Phys. Rev. A **37**, 3909 (1988).

¹³S. J. Linz, M. Lücke, H. W. Müller, and J. Niederländer, Phys. Rev. A **38**, 5727 (1988).

¹⁴Pulses observed most recently in thermally and geometrically very homogeneous cells [P. Kolodner, Phys. Rev. Lett. **66**, 1165 (1991)] are not stationary but have a group velocity that is only slightly smaller than our prediction.

¹⁵M. C. Cross, Phys. Rev. A **38**, 3593 (1988).